Comparison of Pollution Characteristics and Magnetic Response of Heavy Metals in Dustfall before and after COVID-19 Outbreak in Shanghai

Guan Wang [1,2], Qian Xin [1], Xueyu Geng [2], Xinyu Zhu [1], Wen Yao [1], Zhenxiang Ji [1] and Feifan Ren [3,*]

[1] Department of Environment and Architecture, University of Shanghai for Science and Technology, Shanghai 200093, China
[2] School of Engineering, University of Warwick, Coventry CV4 7AL, UK
[3] Key Laboratory of Geotechnical and Underground Engineering of Ministry of Education, Department of Geotechnical Engineering, Tongji University, Shanghai 200092, China
* Correspondence: feifan_ren@tongji.edu.cn

Abstract: In this study, dustfall samples were systematically collected in various regions of Shanghai before and after the occurrence of COVID-19 in December 2019 and December 2020. The magnetic response, content and pollution status of relevant heavy metal elements in the samples were analyzed using environmental magnetism, geochemistry, scanning electron microscopy (SEM) and the enrichment factor (EF) method. The results show that the magnetic particles in the dustfall samples are mainly pseudo-single-domain (PSD) and multi-domain (MD) ferrimagnetic minerals, and Fe, Zn, Cr, and Cu are mainly concentrated in the districts with intensive human activities. Due to restrictions on human activities following the COVID-19 epidemic, both the values of magnetic parameters and the heavy metal pollution level in 2019 are more significant than those in 2020, which is consistent with the Air Quality Index (AQI) results. In addition, magnetic susceptibility (χ_{lf}), non-hysteresis remanence (χ_{ARM}) and saturation isothermal remanence (SIRM) have different degrees of correlation with heavy metal elements, and the correlations with Fe, Pb, Cr and Zn are extremely prominent. The magnetic parameters can effectively and quickly reflect the level of particulate matter pollution, making them a useful tool for monitoring urban air quality.

Keywords: dustfall; environmental magnetism; heavy metal pollution; COVID-19

1. Introduction

With the rapid development of urban and industrial modernization, atmosphere pollution has become one of major environmental issues in Shanghai due to the high energy consumption and explosive growth of vehicle traffic. Particulate matter (PM) is the main component of air pollutants, usually composed of viruses, bacteria, heavy metal carriers, catalysts or reaction beds [1,2]. PM can float into the atmosphere and reach a supersaturated state over a relatively long period, which interferes with various biogeochemical processes and material circulation processes in the surrounding environment [3]. Additionally, the balance of the human respiratory and metabolic systems can be severely disrupted through the food chain. Therefore, air particulate pollution has become a research hotspot in recent years.

Many studies have shown that traditional chemical analysis can effectively evaluate air quality, but it is time-consuming and expensive [4]. Therefore, there is an urgent need to establish an efficient monitoring method to track the spread of urban atmospheric particulate matter, which has very important practical significance for research into solutions for heavy metal pollution in the air [5–7]. As a new type of analysis method, the magnetic approach has been increasingly used in the field of pollution monitoring of environmental carriers, such as urban particulate matter, soil, vegetation, etc., because of its rapid positioning, economic testing, and convenient sampling [8–11]. A large number of studies

have shown that magnetic parameters, such as magnetic susceptibility (χ_{lf}), saturation isothermal remanence (SIRM), and non-hysteresis remanence (χ_{ARM}), are closely related to the concentration of heavy metals in the air. Especially, χ_{lf} and SIRM can be used as effective indicators to evaluate and monitor the level of ferromagnetic particles in the air [8,12,13].

At the end of December 2019, a novel coronavirus (COVID-19) with extremely high contagiosity was firstly reported in Wuhan City and spread rapidly across the world. In order to effectively control the spread of the virus, the Chinese government issued the highest-level emergency response to the epidemic, for example, community blockades, traffic restrictions, public transportation system suspension, the implementation of online offices for factory and corporate personnel, etc. These measures have not only effectively reduced the risk of new coronavirus infections, but also reduced air pollutants generated by industry, vehicle traffic and other factors [14]. Numerous studies have highlighted the positive effects of the COVID-19 lockdown on water and air quality, comparing the percentage of pollutants found before and during the lockdown [15,16]. Scivicco et al. [17] investigated the impact of the COVID-19 pandemic lockdown on the environmental occurrence of eleven heavy metals in the Campania region (Italy) by analyzing bees and bee products.

As one of China's important economic centers and inbound cities, Shanghai is a typical city with rapid urbanization on the east coast and a rapid increase in the number of vehicles, and it was found that there are significant differences in the air PM content with regard to the spatial distribution characteristics of the season [18]. Like other cities, Shanghai has been affected by COVID-19, and human activities have been greatly controlled; however, there are a lack of comparative studies of heavy metal pollution before and after the COVID-19 outbreak. This study aims to better understand the trend of air pollutants before and after the COVID-19 outbreak in Shanghai. For comparison, the sampling cycle was firstly divided into two phases, namely, December 2019 and December 2020, and atmospheric dustfall in various districts was taken as the research medium. Then, using the means of environmental magnetism, geochemistry, scanning electron microscopy (SEM), and the enrichment factor (EF) approach, the pollution characteristics and the magnetic responses of heavy metals in the dustfall samples were investigated, and related analyses were also conducted. The research results can provide data support and theoretical basis for air pollution control in megacities in eastern China.

2. Materials and Methods

2.1. Study Area and Sample Collection

In December 2019 and December 2020, a total of 140 dustfall samples were collected from 14 main administrative districts in Shanghai, including: Yangpu (YP), Hongkou (HK), Huangpu (HP), Jing'an (JA), Xuhui (XH), Pudong (PD), Jiading (JD), Jinshan (JS), Minhang (MH), Songjiang (SJ), Putuo (PT), Fengxian (FX), Changning (CN), Baoshan (BS), Qingpu (QP), and Chongming (CM). These districts cover 5 different functional areas, namely, industrial, transportation, commercial, residential, and clean areas. During the sampling period, it was necessary to meet the basic condition of sunny weather for more than one week. The sampling procedure followed the following three steps [19]. First, plastic brushes, dust buckets and other appliances were used to collect about 10 g of dust from the window sills of buildings exposed to the air at a height of about 1.5 m from the ground. The samples were kept in airtight bags and quickly brought back to the laboratory for later experiments. Second, the samples were put into sealed bags for preservation. Finally, a global positioning system (GPS) was used to record the latitude and longitude of each sample point, and the environmental characteristics of the sampling points was also recorded. The spatial distribution and sampling positions of all sampling points are shown in Figure 1.
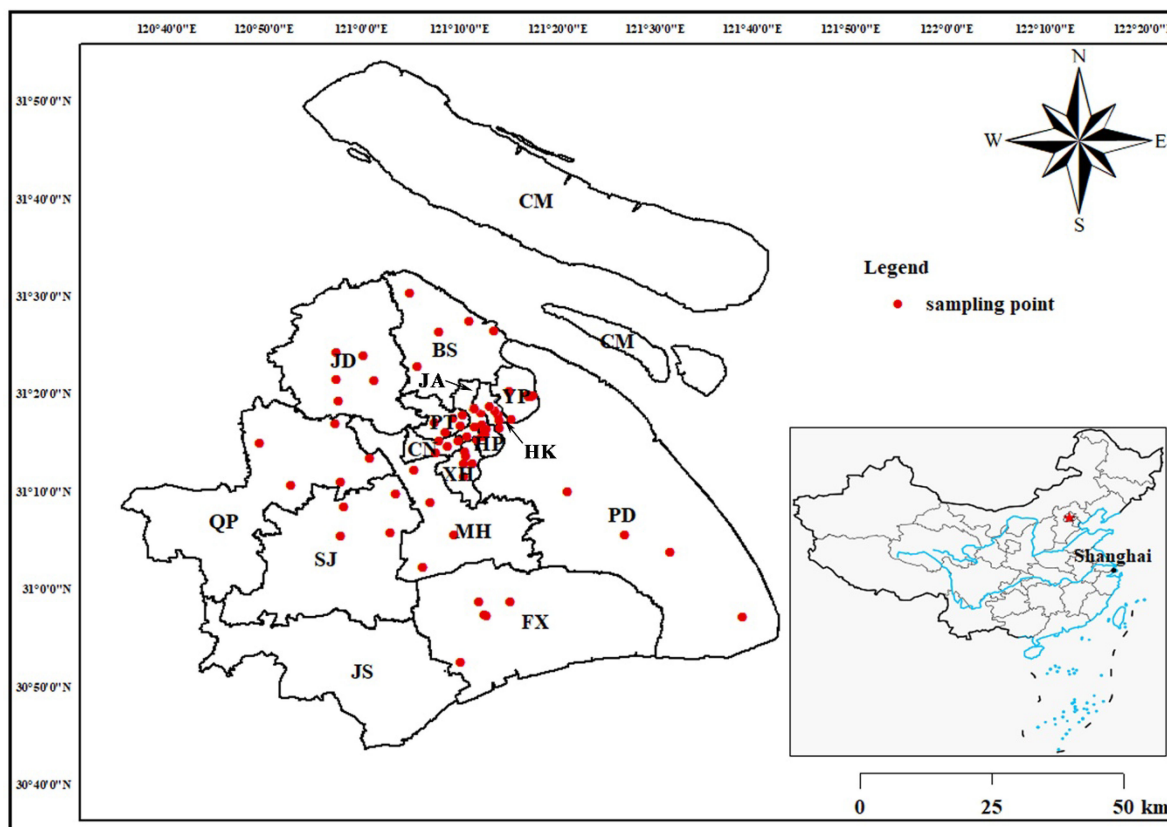
Figure 1. Distribution of sampling points in Shanghai.

2.2. Magnetism Measurement

The air-dried samples were sieved to remove plant debris, hair and other sundries by being passed through a 2 mm nylon sieve, then about 4.0 g of the sample was wrapped with plastic fresh-keeping film, and put it into a cylindrical magnetic special polyethylene sample box for testing. For the duration of the experiment, it is guaranteed that these samples did not contact any other metal materials. All samples were measured with an MS2 susceptibility meter produced by Bartington Company (UK) for obtaining low-frequency magnetic susceptibility (χ_{lf}) and high-frequency magnetic susceptibility (χ_{hf}), and frequency magnetic susceptibility ($\chi_{fd}\%$) can be calculated by $[(\chi_{lf}-\chi_{hf})/\chi_{lf}] \times 100\%$. After demagnetization with an alternating demagnetizer Molspin Detch2000 (UK), the non-hysteresis remanence (ARM) of the sample was measured in a double-speed rotating magnetometer, and χ_{ARM} was calculated. Isothermal remanence (IRM) was measured using an MMPM10 strong magnetometer (UK) and an Argico JR6 rotating magnetometer (Czech Republic). That is to say, for more accurate analysis, the sample was first magnetized under a 1T magnetic field, then the IRM was measured and recorded as saturation isothermal remanence (SIRM), and finally the IRM (-100 mT and -300 mT) in the diamagnetic field was measured. All the magnetic measurements were performed in the State Key Laboratory of Estuarine and Coastal Research, China.

2.3. Metal Measurement

With reference to previous studies [20,21], Graphite Digestion Apparatus was used to digest dust samples in this study. The operation process is as follows: 0.05 g sample was first weighed and put into the digestion tube, and a mixture of nitric acid (HNO$_3$ 5 mL), hydrochloric acid (HCL 5 mL), hydrofluoric acid (HF 5 mL), and perchloric acid (HCLO$_4$ 3 mL) were injected for digestion. The temperature of the graphite digestion apparatus was then adjusted to 180°C, and the digestion tube was sealed and heated for 2 h. After the liquid became a clear and transparent yellow liquid, the power supply was disconnected

and the residual temperature was used to remove the acid. When the liquid temperature dropped to 25 °C, $HNO_3(1\%)$ was employed to take the volume to 50 mL, including rinsing the digestion tank more than 3 times and transferring the rinsing liquid to the collection bottle. Meanwhile, blank samples and Chinese geochemical standard reference samples (GSD-9) were set up for quality assurance and control after digestion. Finally, ICP-OES (Perkin Elmer SCIEX, Optima 8000) was used to test the contents of Cr, Cu, Fe, Mn, Ni, Pb, and Zn metals in the samples.

2.4. Characteristic Analysis of Element Enrichment Factor

The enrichment factor (EF) method was widely adopted to characterize the degree of enrichment of elements in atmospheric particulates, and it can also be used to analyze the sources of different elements in particulates [22,23] and determine the influence of human factors on the concentration of related elements in particulate matter [24]. The calculation formula of EF is expressed as below:

$$EF = \frac{\left(\frac{C_i}{C_r}\right)_{particulate}}{\left(\frac{C_i}{C_r}\right)_{background}} \tag{1}$$

where C_i is the concentration of the i element, and C_r is the concentration of the selected reference element. The enrichment factor can be classified into five levels [25]. When EF < 1, it is indicated that the element in the sample is the natural origin. When the EF values are between 1 and 2, 2 and 5, and 5 and 20, pollution levels are slight, moderate, and significant, respectively. When EF > 20, it means that the element in the sample is extremely polluted as a result of human activities.

2.5. SEM

Some typical samples were selected to analyze the morphological characteristics of dustfall in 2019 and 2020. The selected samples were first adhered to sample holders and gold-plated for pretreatment. A FESEM-4800 scanning electron microscope (SEM), manufactured by Hitachi Co., Ltd., Tokyo, Japan, was then used to observe these typical dustfall samples.

3. Results and Discussion

3.1. Characteristics of Magnetic Parameters

In the application of the environmental magnetism, various environmental magnetism parameters can be comprehensively used to reflect the magnetic properties of matter. In this study, several key magnetic parameters were employed to investigate the particulate pollution. Among them, χ_{lf} generally indicates the distribution characteristics of the magnetic mineral content in the sample. SIRM is related to the total remanence-carrying minerals and controlled largely by stable single-domain (SSD) ferrimagnetic grain concentrations and the presence of canted antiferromagnetic minerals [26,27]. χ_{ARM} is generally particularly sensitive to single-domain particles (SD) and PSD particles, and is generally used to reflect the magnetic domain properties of magnetic particles [28–30]. HIRM is generally used to reflect the relative content changes of ferrimagnetic minerals and incomplete antiferromagnetic minerals.

Table 1 shows the magnetic measurement results of samples before and after the COVID-19 outbreak. The magnetic parameters of the dustfall in December 2019 (before COVID-19 outbreak) are generally higher than those in December 2020 (after COVID-19 outbreak). The mean value of χ_{lf} is 718.521×10^{-8} m^3/kg in 2019 and 672.071×10^{-8} m^3/kg in 2020, ranging from 54.950×10^{-8} m^3/kg to 2374.250×10^{-8} m^3/kg in 2019 and 100.105×10^{-8} m^3/kg to 3386.369×10^{-8} m^3/kg in 2020. It is indicated that the magnetic minerals of the samples before and after the epidemic were mainly made of ferromagnetic minerals. The mean value of SIRM is $92,992.646 \times 10^{-5}$ Am^2/kg in 2019 and $56,255.653 \times 10^{-5}$ Am^2/kg in 2020, ranging from 8517.054×10^{-5} Am^2/kg to $225,487.342 \times 10^{-5}$ Am^2/kg in 2019, and

from 41.813×10^{-5} Am^2/kg to $191{,}278.250 \times 10^{-5}$ Am^2/kg in 2020. SIRM values in 2019 and 2020 are both higher than the background value (237.100×10^{-5} Am^2/kg), reflecting the high degree of ferrimagnetic mineral spatial enrichment in the samples before and after COVID-19 outbreak. The mean value of χ_{ARM} is 1295.862×10^{-8} m^3/kg in 2019 and 880.937×10^{-8} m^3/kg in 2020, ranging from 148.743×10^{-8} m^3/kg to 3485.171×10^{-8} m^3/kg in 2019 and 23.787×10^{-8} m^3/kg to 4592.721×10^{-8} m^3/kg in 2020. The mean value of HIRM is 1842.538×10^{-8} m^3/kg in 2019 and 368.269×10^{-8} m^3/kg in 2020, ranging from 48.060×10^{-5} Am^2/kg to $25{,}925.123 \times 10^{-5}$ Am^2/kg in 2019 and 44.473×10^{-5} Am^2/kg to 1137.701×10^{-5} Am^2/kg in 2020. Thus, it can be concluded that the magnetic properties of dustfall in Shanghai were dominated by both ferromagnetic minerals and incomplete antiferromagnetic minerals [8].

Table 1. Magnetic measurement results of samples before and after COVID-19 outbreak.

	χ_{lf} (10^{-8} m^3/kg)	χ_{fd}%	χ_{ARM} (10^{-8} m^3/kg)	SIRM (10^{-5} Am^2/kg)	HIRM (10^{-5} Am^2/kg)	χ_{ARM}/χ_{lf}	χ_{ARM}/SIRM (10^{-3} mA^{-1})
Range	54.950~2374.250	0.081~43.737	148.743~3485.171	8517.054~225,487.342	48.060~25,925.123	0.640~3.722	0.002~0.038
	100.105~3386.369	0.775~26.480	23.787~4592.721	41.813~191,278.250	44.473~1137.701	0.007~4.392	0.001~14.401
Mean	718.521	4.354	1295.862	92,992.646	1842.538	1.950	0.015
	672.017	4.392	880.937	56,255.653	368.269	1.437	0.222
Median	597.224	2.825	1088.586	73,628.214	944.866	1.826	0.014
	574.541	2.524	679.978	47,373.563	353.007	1.443	0.014
SD	427.320	5.872	744.207	50,104.971	3623.146	0.582	0.006
	517.162	4.427	776.471	37,426.130	216.888	0.795	1.719
Background [31]	29.100 ± 9.800	2.100	103.300	237.100	34.400	3.550	0.436

Note: The gray parts represent 2019, the white parts represent 2020.

Furthermore, when the concentration of MD and PSD grains dominates in dust (between 5% and 6%), and there are no existent SP grains, $\chi_{fd}\%$ can be used to represent the concentration of MD and PSD grains [32–34]. When $\chi_{fd}\% > 10\%$, it is suggested that there are a significant number of SP particles [35]. In this study, the mean value of $\chi_{fd}\%$ is 4.354 in 2019 and 4.392 in 2020, both less than 5%, and when combined with the median values (2.825 in 2019 and 2.524 in 2020) and $\chi_{fd}\%$ background value (2.100) [31], it is indicated that MD and PSD grains constitute the majority of ferromagnetic mineral grains.

The ratio of the magnetic parameters mainly reflects the grain size of the magnetic minerals. The ratios of χ_{ARM}/χ_{lf} and $\chi_{ARM}/SIRM$ can signify the grain size of magnetic minerals, which decrease with the increase in grain size [27]. χ_{ARM}/χ_{lf} indicates the size of ferromagnetic mineral particles, with higher ratios reflecting more SSD particles and lower ratios indicating more MD or superparamagnetic particles (SP) [26,36]). $\chi_{ARM}/SIRM$ also indicates the particle size variation of magnetic particles, with lower ratios reflecting more PSD and MD particles [37]. The mean values of χ_{ARM}/χ_{lf} are 1.950 in 2019 and 1.437 in 2020. The difference between the χ_{ARM}/χ_{lf} values before and after the COVID-19 outbreak is slight, showing the particle size in 2020 as slightly coarser than that in 2019. In addition, the χ_{ARM}/χ_{lf} values of the dustfall are significantly lower than the background value (3.550) [31], indicating that the grain size of the magnetic particles in the dustfall is significantly coarser. In addition, the mean values of $\chi_{ARM}/SIRM$ are 0.015×10^{-3} m/A in 2019 and 0.222×10^{-3} m/A in 2020, both of which are lower than the background value (0.240×10^{-3} m/A) [31]. In conclusion, the mean values of χ_{ARM}/χ_{lf} and $\chi_{ARM}/SIRM$ of the samples are less than 10 and 0.50×10^{-3} m/A, respectively, indicating that the ferrimagnetic minerals are dominated by PSD and coarser MD grains in the study area.

Figure 2 shows the Dearing plot and King plot of the dustfall [32,38]. Among them, the relationship diagram of χ_{ARM} and χ_{lf} (as shown in Figure 2a) was mainly used for analyzing the particle size distribution characteristics of the samples [26,27]. The values of $\chi_{fd}\%$ and $\chi_{ARM}/SIRM$ of the dustfall samples in 2019 and 2020 fall within the range of PSD and MD, and the largest part of the SP particle fraction is less than 50%. Both the Dearing plot and King plot prove that the magnetic particles in the study (before and after COVID-19 outbreak) are mainly PSD and MD magnetic particles with relatively coarse particle size, and the volume fraction of SP particles is mostly less than 50%.
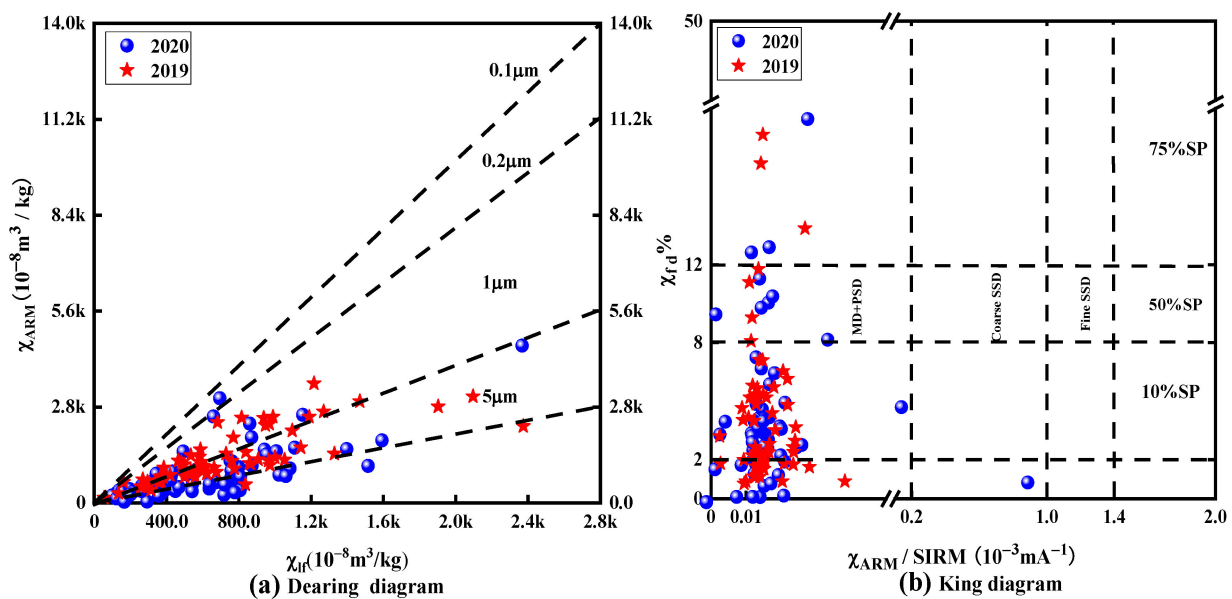

Figure 2. Dearing and King plot of dustfall [26,32].

In summary, it can be concluded that the average values of the magnetic parameters (χ_{ARM}, SIRM, HIRM) before the epidemic (in 2019) are generally higher as a whole, which is

consistent with previous research conclusions [39]. Additionally, the average Air Quality Index (AQI) in December 2019 (AQI_{2019} = 69) and in December 2020 (AQI_{2020} = 68) in Shanghai [40] shows the same trend as the magnetic parameters in this study. There is a significant change trend between the magnetic parameter values and the concentration of magnetic particles after the epidemic. This further confirms that the interference of the external environment has a negative impact on the changes in magnetic parameters [39,41,42]. There may be two factors for this temporal variation. On the one hand, man-made activities were obviously restricted after the epidemic, and the flow of people and vehicles was reduced to a certain extent, leading to a decrease in the content of magnetic particles and the magnetic parameter values in 2020. On the other hand, it is most likely due to the "Three-year plan on defending the blue sky" issued by the State Council in 2018 [43], which has made a significant contribution to exploring how to achieve coordinated control of the types of air pollutants and the content of air pollutants at the city level, and to speed up the improvement of ambient air quality to win the "Blue Sky Defense". On the whole, the magnetic results demonstrate that ferrimagnetic minerals dominated the magnetism of dust produced by human activities. This is further evidence that the significant differences in air quality before and after the COVID-19 outbreak may be related to anthropogenic activities.

3.2. Temporal and Spatial Variation Characteristics of Magnetic Parameters of Dustfall

Figure 3 shows the variation characteristics of the magnetic parameters of the samples in different districts before and after the COVID-19 outbreak. It can be seen that the mean values of χ_{lf}, χ_{ARM}, SIRM, $\chi_{ARM}/SIRM$, χ_{ARM}/χ_{lf}, and $\chi_{ARM}/\chi_{fd}\%$ in 2019 are clearly higher than those in 2020. Spatially, the peaks of χ_{lf}, χ_{ARM}, and SIRM of the samples in December 2019 are mainly concentrated in the downtown areas with more human activities, higher human flow and denser vehicle flow (car parts wear, exhaust emissions, etc.), such as the XH, PD, PT, and CN districts. As a whole, the spatial distribution of the ferromagnetic mineral content of the dustfall in Shanghai is extremely uneven. The content of ferromagnetic minerals near the city center is higher, and the suburban area is generally lower. The distribution trends of $\chi_{ARM}/SIRM$ and χ_{ARM}/χ_{lf} parameters are similar; that is, the higher values are mainly concentrated in the XH, PD, PT, and SJ districts. The peaks of χ_{lf}, χ_{ARM}, and SIRM of the samples in 2020 are mainly concentrated in the HP, PD, PT, CN, and BS districts. Compared with 2019, for magnetic parameters describing the properties of particles, the three magnetic parameters of the dustfall samples in 2020 have a wider spatial span, which further characterizes that the closer to the city center, the higher the enrichment degree of ferromagnetic minerals. For the magnetic ratio parameters describing the particle size, the peaks of χ_{ARM}/χ_{lf} and $\chi_{ARM}/SIRM$ are mainly concentrated in the PT, XH, and CN districts. The $\chi_{ARM}/\chi_{fd}\%$ value fluctuates slightly, but there is still a significantly higher value in the PT area.

Based on the above magnetic analysis, it can be further found that PSD magnetic particles and MD magnetic particles, mainly from human activities such as high human flow and dense vehicle flow (car parts wear, exhaust emissions, etc.), are the dominant magnetic minerals [36,44,45]. In terms of time, the content of magnetic minerals in 2019 is higher than that in 2020. It is speculated that, with the effective implementation of the "Three-year plan on defending the blue sky" and travel restriction policies, the flow of people and vehicles were decreased in 2020.
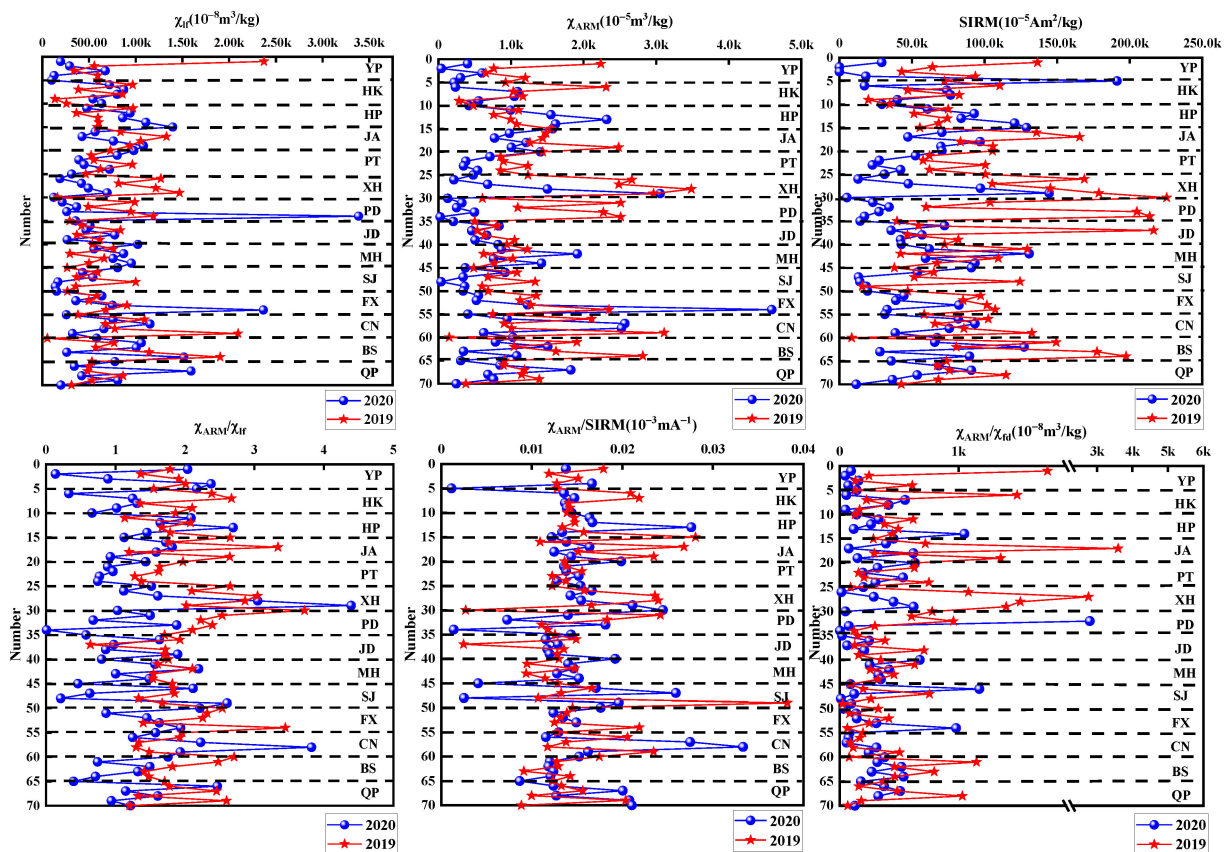
Figure 3. Temporal and spatial distribution characteristics of the magnetic parameters.

3.3. Analysis of Heavy Metal Content

Dustfall has an extremely complex composition of chemical elements due to its source, migration and transformation processes, and sedimentation processes [12], and it often contains a large number of metal elements [44,46,47].

Table 2 shows the contents of the metal elements in the dustfall and background samples [48]. The Fe and Zn contents are the highest in the samples of 2019, with average values of 22,2859.800 mg/kg and 2933.821 mg/kg, respectively. The average value of Mn is 784.988 mg/kg. The elements of Cr, Cu, and Pb are similar in content, with the average values being 220.456 mg/kg, 222.860 mg/kg, and 229.604 mg/kg, respectively, and there are obviously larger and different fluctuation ranges. The content of Ni is the lowest, with an average value of 65.126 mg/kg. Therefore, the extremely high content of Fe and Ni can be corroborated by the preliminary conclusions of the high content of ferromagnetic minerals in the samples of December 2019. In the samples of December 2020, the contents of Fe and Cu elements are also relatively high, with average values of 711.668 mg/kg and 143.528 mg/kg, respectively. The contents of Pb, Ni, and Zn are similar, with the average values being 100.813 mg/kg, 98.152 mg/kg, and 91.343 mg/kg, respectively. The Cr element content is the lowest, with the average value of 43.615 mg/kg. From the perspective of the overall change trend, it can be found that the metal content of the samples in 2019 is higher than that in 2020. In addition, all the samples in 2019 and 2020 contain a large amount of Fe, Ni, and Cu.

Table 2. Heavy metal element content in dustfall.

mg/kg	Cr	Cu	Fe	Mn	Ni	Pb	Zn
Range	58.333~823.500	41.667~473.500	11,032.180~58,955.220	243.158~1941.250	7.632~354.500	1468.000~16.905	16,334.211~321.429
	133.333~26.944	4425.863~1.003	4801.527~54.962	401.230~20.565	107.995~89.077	140.564~84.480	403.501~0.280
Mean	220.456	222.860	35,388.384	784.988	65.126	229.604	2933.821
	43.615	143.528	711.668	74.157	98.152	100.813	91.343
Median	193.250	213.233	36,762.500	762.171	60.451	144.092	2321.264
	31.944	85.340	326.272	28.427	98.142	98.236	67.087
SD	120.314	106.190	8569.914	284.969	49.197	232.385	2754.331
	23.259	517.181	984.392	85.840	2.119	8.273	88.881
Background [48]	179.680	128.730	40,695.000	902.400	4679.790	812.360	2112.580

Note: The gray parts represent 2019, the white parts represent 2020.

Figure 4 shows the variation characteristics of the heavy metal content of the samples in different districts before and after COVID-19 outbreak. The peak values of heavy metal elements Fe, Zn, and Cu in 2019 are mainly concentrated in downtown areas such as the BS, XH, HP, and CN districts. Among them, Fe elements may come from soil, metal smelting, and brake pad wearing [49]. Cu and Zn elements may come from traffic emissions, such as automobile fuel, galvanized materials, the use of zinc compounds in rubber products, the consumption of vehicle tires and exhaust, gas, etc. [49–51]. The high values of Fe, Zn, and Cu in the study area are mainly due to the large flow of people, the denser traffic, and the burning of gasoline. The contents of Mn, Cr, and Pb are relatively distributed with a slight fluctuation range, and mainly concentrated in downtown areas, such as the BS (which was an industrial area before 2017), XH, and CN districts which are areas with high traffic flow and intensive human activities (industrial waste gas, motor vehicle exhaust, and building dust). Cr, Pb, and Mn elements may derive from the wear of brake pads, tires, or other components [52]. The results further verify that human activities (metal manufacturing, steel production, smelting activities) have a significant interference effect on the enrichment effect of metals. Additionally, the pollution changed from single stable pollution to compound pollution. The high contents of Fe, Zn, and Cu elements in the samples of December 2020 were mainly concentrated in the YP, HK and HP districts, mainly due to the fact that these areas are located close to the central ring of Shanghai, with more residential areas and relatively frequent human activities. The contents of Mn, Cr, and Pb show a basically similar spatial distribution trend, and the contents of the samples in the downtown area such as the YP, HK, HP, and XH districts are significantly higher than those in other regions with less human activities. It can be seen that human factors have a certain influence on the heavy metal pollution of particulate matter.
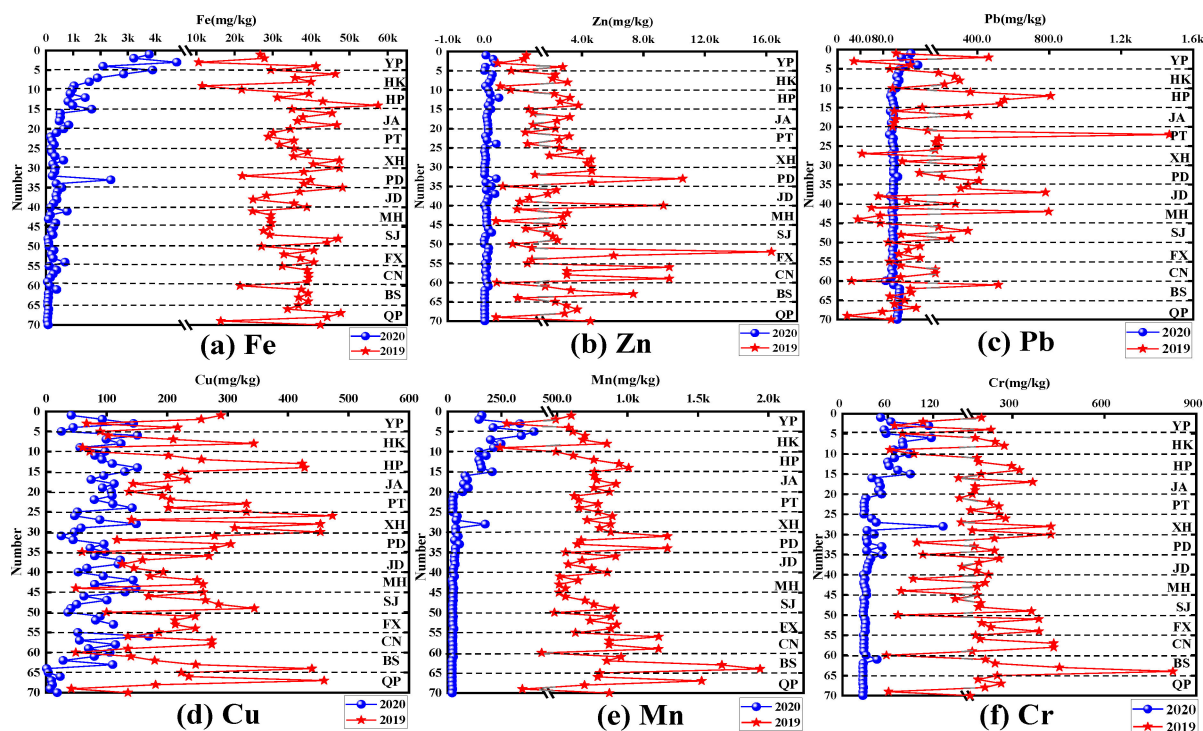

Figure 4. Spatial variation characteristics of the heavy metal content before and after COVID-19 outbreak.

Combining the element measurement results of the dust samples in 2019 and 2020, it can be found that the metal element contents in 2019 (before COVID-19) are significantly higher than those in 2020 (after COVID-19 outbreak). For instance, the concentrations of Fe, Cr, Cu, and Zn in 2019 are significantly higher than those in 2020, and in particular, the Fe content changes significantly before and after the epidemic occurrence. It is further proved

that the significant difference in air quality before and after COVID-19 outbreak is likely to be closely related to human activities, for example, human activities were obviously restricted after the epidemic and the flow of people and vehicles were reduced to a certain extent, resulting in the relative weakening of heavy metal pollution. Moreover, the district variation trends of the metal content in the samples of 2019 and 2020 are basically similar; especially, Fe, Cu and Zn are the most important pollution elements, and their peaks are mainly concentrated in the PT, XH, HP districts due to various human activities. However, the contents of Mn, Cr, and Zn metals showed a spatially different distribution, which was most likely caused by the impact of COVID-19 on human activities, such as industrial action and transportation in space [53]. On the whole, the heavy metal contents of the dustfall in 2019 were higher than those in December 2020. Based on the district distribution characteristics of the heavy metals, it is further confirmed that the pollution status of the downtown areas (PT, HP, XH, PD) is significantly higher than that in the suburbs. The closer to the downtown area, the greater the traffic volume, the greater the proportion of human influence factors, and the more obvious the degree of disturbance to the environment, further indicating that the degree of heavy metal pollution is closely related to human factors. This conclusion is highly consistent with the district distribution characteristics of the magnetic parameters; that is, particle magnetic domain size, particle type, metal content, and type are all closely related to human activities.

3.4. Characteristic Analysis of the Enrichment Factor of the Elements (EF)

The enrichment factor has been widely used to evaluate the pollution degree of heavy metals in particulate matter and the influence of human factors in many studies [54,55], and it was found that Fe, Pb, Cr, V, Ni, Zn, and other elements are highly enriched in particles, and most of them come from human activities.

In this study, Mn was selected as the reference element in the EF calculation, and the pollution enrichment characteristic factors of Cr, Cu, Fe, Pb, and Zn were analyzed in the atmospheric dust before and after the epidemic occurrence. The EF values of the elements are shown in Table 3. The EF value of Fe in the samples of December 2019 is the highest (EF = 18.120), and it is obviously higher than that (EF = 4.302) in the samples of December 2020, indicating that Fe pollution is extremely significant, mainly due to the more intense human activities before the COVID-19 outbreak. In addition, the EF values of Zn in the dustfall samples of December 2019 and December 2020 are relatively high, reaching 4.732 and 1.560, respectively. The EF value of Zn in 2019 was more significant than that in 2020, indicating that the Zn pollution was significant in 2019, mainly coming from intense human activities, such as metal material manufacturing, fuel combustion, and transportation before the COVID-19 epidemic. The EF values of Cu, Ni, and Pb in the dustfall samples of 2019 and 2020 are all less than 1, indicating that the metal elements' pollution caused by human activities is extremely low.

Table 3. Enrichment factor of metals.

EF Value	Mn	Cr	Cu	Fe	Ni	Pb	Zn
2019	1.000	0.218	0.037	18.120	0.020	0.058	4.732
2020	1.000	0.456	0.253	4.302	0.289	0.270	1.560

In summary, the enrichment levels of Fe and Zn elements in the dustfall of 2019 are significantly higher than those of 2020, indicating heavy Fe pollution and moderate Zn pollution before the COVID-19 outbreak, and moderate Fe pollution and mild Zn pollution after the COVID-19 outbreak. Through comparing the EF values of the samples in 2019 and 2020, it can be seen that the enrichment factor values of the heavy elements in 2019 are significantly greater than those in 2020, which is likely due to the execution of air pollution management regulations and the reduction in human activities during the

COVID-19 epidemic. The EF calculation results in 2019 are similar to the results of previous studies [56].

3.5. Analysis of Particle Morphology Characteristics

Scanning electron microscopy (SEM) can be directly used to obtain the morphology of dustfall and subsequently analyze the mineral composition of a single particle, which can provide not only information on its source, but also an important method to understand atmospheric chemical reactions [57].

Figure 5 shows the electronic images of typical dustfall samples in 2019 and 2020. It can be found that there were significant differences in the dustfall samples before and after the epidemic's occurrence. The particle shapes can be generally classified as spherical and massive particulates. The morphology of the typical dustfall samples in 2019 is shown in Figure 5a. The particles of the YP district are mainly spherical and massive, most likely due to industrial activity products of high temperature processes such as metal smelting and cement [58]. The particle appearance of the dustfall sample in the JA district (a typical residential district) is mainly elongated shapes. This phenomenon is most likely caused by frequent local building construction [59]. The particle appearance in the dustfall sample of the XH district (a typical industrial district) shows blocky and irregular shapes, which may be due to the interference of road dust [52]. The dustfall sample in the BS district (a typical industrial district) has a mostly columnar morphology, further indicating the significant impact of industrial activities. In addition, the SEM characteristics of typical dustfall samples in 2020, sharing the same locations with the samples in 2019, are shown in Figure 5b. The particle appearances of the dustfall samples in different districts are spherical, massive, and have a few irregularities as a whole. The spherical shape is the most prominent, indicating the significant impact from human activities, such as building dust and automobile exhaust emissions. In summary, the morphological characteristics of the dustfall samples in 2019 and 2020 are mainly dominated by road dust, intensive traffic, and the impact of nearby construction, and part of the pollution comes from natural pollution sources such as soil or rock weathering dust. Significantly, compared with 2020, the morphological types of dustfall samples in 2019 are more extensive and characteristic, indicating that the forms of human activities were more diverse before the epidemic.
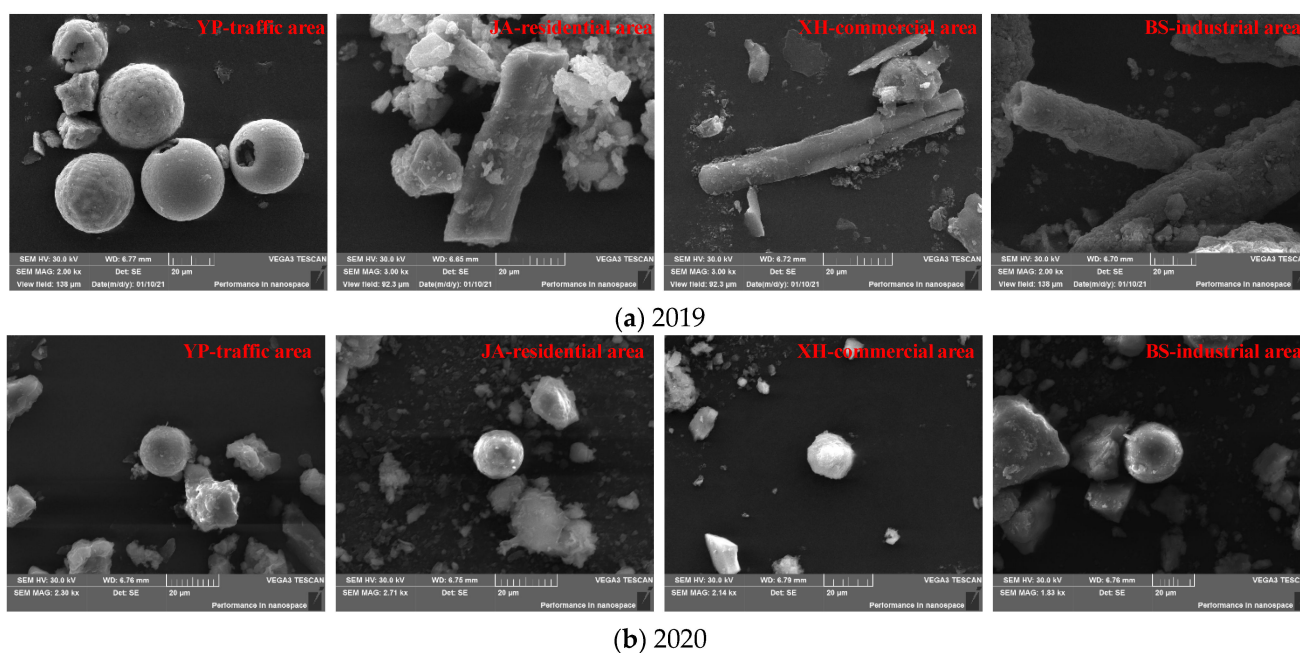

(**a**) 2019

(**b**) 2020

Figure 5. Morphology characteristics of typical dustfall samples.

3.6. Correlation Analysis of Heavy Metal Elements and Magnetic Parameters

In order to comprehensively analyze the correlation between the magnetic parameters and the content of heavy metals in the dustfall samples in Shanghai, SPSS 22 software was employed for multivariate statistical analysis.

Table 4 shows the summary of Spearman coefficients of metal and magnetic parameters. χ_{lf} is significantly positively correlated with Fe and Pb in 2019, and the correlation coefficients are 0.554 and 0.716, respectively. The ratio parameters χ_{ARM}/χ_{lf}, χ_{ARM}/χ_{fd} and $\chi_{ARM}/SIRM$ are significantly related to the correlation of each element (0.270 < R < 0.935). In the results of the correlation analysis of 2020, χ_{ARM} and SIRM have extremely significant correlations with Cr, Fe, Mn, Ni, and Pb (0.521 < R < 0.997). The ratio parameters χ_{ARM}/χ_{lf}, χ_{ARM}/χ_{fd}, $SIRM/\chi_{lf}$, and $\chi_{ARM}/SIRM$ have different correlation degrees with each heavy metal, ranging from 0.229 to 0.890. Especially, the correlation with Fe, Pb and Zn is particularly prominent (R > 0.625). These conclusions are consistent with those of the characteristic analysis of the magnetic parameters and the enrichment factor of the elements stated above.

Table 4. Summary of Spearman coefficients of metal and magnetic parameters (N = 140).

Parameter	Cr	Cu	Fe	Mn	Ni	Pb	Zn
χ_{lf}	0.013	0.015	0.554 **	0.001	0.037	0.716 **	0.004
	0.378 *	0.009	0.139 *	0.420*	0.048	0.300 *	0.070
χ_{ARM}	0.016	0.020	0.018	0.001	0.040	0.801 **	0.007
	0.826 **	0.001	0.989 **	0.801 **	0.522 **	0.137	0.034
SIRM	0.002	0.003	0.123	0.002	0.008	0.674 **	0.001
	0.958 **	0.089	0.799 **	0.814 **	0.827 **	0.574 **	0.240 *
χ_{ARM}/χ_{lf}	0.777 **	0.874 **	0.001	0.997 **	0.816 **	0.551 **	0.916 **
	0.563 **	0.453 *	0.411 *	0.559 **	0.304 *	0.629 **	0.369 *
χ_{ARM}/SIM	0.935 **	0.735 **	0.458 *	0.422	0.916 **	0.564 **	0.748 **
	0.353 *	0.474 *	0.577 **	0.229 *	0.388 *	0.116 *	0.890 **
χ_{ARM}/χ_{fd}	0.664 **	0.270 *	0.625 **	0.281 *	0.674 **	0.793 **	0.151
	0.072	0.761 **	0.313 *	0.039	0.735 **	0.678 **	0.792 **

Note: N = 140; ** correlation is significant at the 0.01 level (two-tailed); * correlation is significant at the 0.05 level (two-tailed). The gray parts represent 2019, the white parts represent 2020.

Combining the correlation results of the magnetic parameters and the metal contents in 2019 and 2020, it can be found that Cu, Fe, Mn, Zn had significant correlations with χ_{lf}, χ_{ARM}, SIRM, χ_{ARM}/χ_{lf}, χ_{ARM}/χ_{fd}, and $\chi_{ARM}/SIRM$. Pollutants such as ferromagnetic minerals produced by human activities are interdependent on heavy metals, and iron–manganese oxides largely control the geochemical cycles of metal elements [6]. These conclusions are similar to previous studies [60,61].

4. Conclusions

COVID-19 has had an impact on urban particulate pollution, as well as people's lives. In this study, samples obtained before and after the COVID-19 outbreak in Shanghai were subjected to magnetic, chemical, and scanning electron microscopy investigation. The pollution characteristics and the magnetic responses of heavy metals were compared and studied. The main conclusions are as follows:

1. PSD and MD ferrimagnetic minerals predominate in the dustfall in Shanghai. The dustfall samples in 2019 had a higher magnetic mineral concentration than those in 2020. Magnetic parameter peaks are concentrated in the districts of XH, CN, and BS, which have high levels of population mobility, heavy industrial activity, and significant traffic flow. The epidemic prevention and control measures had a significant impact on the magnetic characteristics of the dustfall.

2. Fe has the largest concentration of heavy metals, followed by Pb, Zn, Mn, and Cu. Due to constraints on human activity following the COVID-19 epidemic, the metal composition of the dustfall samples in 2020 is much lower than that of 2019. This

directly correlates to a relative weakening of metal pollution. Moreover, since Fe, Zn, Cr and Cu are concentrated in areas of intense human activity, such as BS, HP, and CN, heavy metal pollution is more severe in these areas.

3. χ_{lf}, χ_{ARM} and SIRM before and after COVID-19 outbreak have different correlations with Cr, Fe, Zn, Pb, Mn, and Cu. The contents of Fe, Pb, Cr, and Zn are significantly correlated with the magnetic parameters, further proving the indication of magnetic parameters on the heavy metal pollution of atmospheric particulate matter.

4. Although this study compared the contamination characteristics and magnetic responses of heavy metals in fallout before and after the COVID-19 outbreak in Shanghai, the sampling density is still not high and the testing means are limited, and it is proposed to take additional samples and adopt more testing and analytical means to analyze and study the samples subsequently.

Conflicts of Interest: The authors declare no conflict of interest.

References

1. Ming, L.; Jin, L.; Li, J.; Fu, P.Q.; Yang, W.Y.; Liu, D.; Zhang, G.; Wang, Z.F.; Li, X.D. PM2. 5 in the Yangtze River Delta, China: Chemical compositions, seasonal variations, and regional pollution events. *Environ. Pollut.* **2017**, *223*, 200–212. [CrossRef] [PubMed]
2. Zhang, J.; Liu, L.; Xu, L.; Lin, Q.H.; Zhao, H.J.; Wang, Z.B.; Guo, S.; Hu, M.; Liu, D.T.; Shi, Z.B.; et al. Exploring wintertime regional haze in northeast China: Role of coal and biomass burning. *Atmos. Chem. Phys.* **2020**, *20*, 5355–5372. [CrossRef]
3. Li, Z.Y.; Ma, Z.W.; van der Kuijp, T.J.; Yuan, Z.W.; Huang, L. A review of soil heavy metal pollution from mines in China: Pollution and health risk assessment. *Sci. Total Environ.* **2014**, *468*, 843–853. [CrossRef] [PubMed]
4. Guo, H.; Gu, X.F.; Ma, G.X.; Shi, S.Y.; Wang, W.N.; Zuo, X.; Zhang, X.C. Spatial and temporal variations of air quality and six air pollutants in China during 2015–2017. *Sci. Rep.* **2019**, *9*, 15201. [CrossRef] [PubMed]
5. Sun, X.; Li, H.M.; Guo, X.; Sun, Y.K.; Li, S.M. Capacity of six shrub species to retain atmospheric particulates with different diameters. *Environ. Sci. Pollut. Res.* **2018**, *25*, 2643–2650. [CrossRef]
6. Wang, G.; Chen, J.; Zhang, W.; Ren, F.F.; Chen, Y.Y.; Fang, A.D.; Ma, L.J. Magnetic properties of street dust in Shanghai, China and its relationship to anthropogenic activities. *Environ. Pollut.* **2019**, *255*, 113214. [CrossRef]
7. Wang, B.; Zhang, X.C.; Zhao, Y.H.; Zhang, M.; Jia, J. Spatial and Temporal Distribution of Pollution Based on Magnetic Analysis of Soil and Atmospheric Dustfall in Baiyin City, Northwestern China. *Int. J. Environ. Res. Public Health* **2021**, *18*, 1681. [CrossRef]
8. Yang, T.; Liu, Q.; Li, H.; Zeng, Q.L.; Chan, L.S. Anthropogenic magnetic particles and heavy metals in the road dust: Magnetic identification and its implications. *Atmos. Environ.* **2010**, *44*, 1175–1185. [CrossRef]
9. Bourliva, A.; Kantiranis, N.; Papadopoulou, L.; Aidona, E.; Christophoridis, C.; Kollias, P.; Evgenakis, M.; Fytianos, K. Seasonal and spatial variations of magnetic susceptibility and potentially toxic elements (PTEs) in road dusts of Thessaloniki city, Greece: A one-year monitoring period. *Sci. Total Environ.* **2018**, *639*, 417–427. [CrossRef]
10. Dytłow, S.; Winkler, A.; Górka-Kostrubiec, B.; Sagnotti, L. Magnetic, geochemical and granulometric properties of street dust from Warsaw (Poland). *J. Appl. Geophys.* **2019**, *169*, 58–73. [CrossRef]
11. Ma, X.; Jia, H.; Sha, T.; An, J.L.; Tian, R. Spatial and seasonal characteristics of particulate matter and gaseous pollution in China: Implications for control policy. *Environ. Pollut.* **2019**, *248*, 421–428. [CrossRef]
12. Wang, G.; Chen, J.; Zhang, W.; Chen, Y.Y.; Ren, F.F.; Fang, A.D.; Ma, L.J. Relationship between magnetic properties and heavy metal contamination of street dust samples from Shanghai, China. *Environ. Sci. Pollut. Res.* **2019**, *26*, 8958–8970. [CrossRef]

13. Aguilera, A.; Morales, J.J.; Goguitchaichvili, A.; García-Oliva, F.; Armendariz-Arnez, C.; Quintana, P.; Bautista, F. Spatial distribution of magnetic material in urban road dust classified by land use and type of road in San Luis Potosí, Mexico. *Air Qual. Atmos. Health* **2020**, *13*, 951–963. [CrossRef]

14. Zheng, H.; Kong, S.; Chen, N.; Yan, Y.Y.; Liu, D.T.; Zhu, B.; Xu, K.; Cao, W.X.; Ding, Q.Q.; Lan, B.; et al. Significant changes in the chemical compositions and sources of PM2. 5 in Wuhan since the city lockdown as COVID-19. *Sci. Total Environ.* **2020**, *739*, 140000. [CrossRef]

15. Zambrano-Monserrate, M.A.; Ruano, M.A.; Sanchez-Alcalde, L. Indirect effects of COVID-19 on the environment. *Sci. Total Environ.* **2020**, *728*, 138813. [CrossRef]

16. Elsaid, K.; Olabi, V.; Sayed, E.T.; Wilberforce, T.; Abdelkareemd, M.A. Effects of COVID-19 on the environment: An overview on air, water, wastewater, and solid waste. *J. Environ. Manag.* **2021**, *292*, 112694. [CrossRef]

17. Scivicco, M.; Nolasco, A.; Esposito, L.; Ariano, A.; Squillante, J.; Esposito, F.; Cirillo, T.; Severino, L. Effects of COVID-19 pandemic lockdown and environmental pollution assessment in Campania region (Italy) through the analysis of heavy metals in honeybees. *Environ. Pollut.* **2022**, *307*, 119504. [CrossRef]

18. Shu, L.; Xie, M.; Gao, D.; Wang, T.J.; Fang, D.X.; Liu, Q.; Huang, A.N.; Peng, L.W. Regional severe particle pollution and its association with synoptic weather patterns in the Yangtze River Delta region, China. *Atmos. Chem. Phys.* **2017**, *17*, 12871–12891. [CrossRef]

19. Hanesch, M.; Scholger, R.; Rey, D. Mapping dust distribution around an industrial site by measuring magnetic parameters of tree leaves. *Atmos. Environ.* **2003**, *37*, 5125–5133. [CrossRef]

20. Rauret, G. Extraction procedures for the determination of heavy metals in contaminated soil and sediment. *Talanta* **1998**, *46*, 449–455. [CrossRef]

21. Voica, C.; Dehelean, A.; Maria, A.; Geana, I. Method validation for determination of metals in soils by ICP-MS. *Rom. Rep. Phys.* **2012**, *64*, 221–231.

22. Kaushik, A.; Kansal, A.; Santosh; Meena; Kumari, S.; Kaushik, C.P. Heavy metal contamination of river Yamuna, Haryana, India: Assessment by metal enrichment factor of the sediments. *J. Hazard. Mater.* **2009**, *164*, 265–270. [CrossRef] [PubMed]

23. Ghrefat, H.A.; Abu-Rukah, Y.; Rosen, M.A. Application of geoaccumulation index and enrichment factor for assessing metal contamination in the sediments of Kafrain Dam, Jordan. *Environ. Monit. Assess.* **2011**, *178*, 95–109. [CrossRef] [PubMed]

24. Zoller, W.; Gladney, E.; Duce, R. Atmospheric concentrations and sources of trace metals at the South Pole. *Science* **1974**, *183*, 198–200. [CrossRef] [PubMed]

25. Duce, R.A.; Hoffman, G.L.; Zoller, W.H. Atmospheric trace metals at remote northern and southern hemisphere sites: Pollution or natural? *Science* **1975**, *187*, 59–61. [CrossRef]

26. King, J.; Banerjee, S.K.; Marvin, J.; Özdemir, Ö. A comparison of different magnetic methods for determining the relative grain size of magnetite in natural materials: Some results from lake sediments. *Earth Planet. Sci. Lett.* **1982**, *59*, 404–419. [CrossRef]

27. Hay, K.L.; Dearing, J.A.; Baban, S.M.J.; Loveland, P. A preliminary attempt to identify atmospherically-derived pollution particles in English topsoils from magnetic susceptibility measurements. *Phys. Chem. Earth* **1997**, *22*, 207–210. [CrossRef]

28. Thompson, R.; Stober, J.C.; Turner, G.M.; Oldfield, F.; Bloemendal, J.; Dearing, J.A.; Rummery, T.A. Environmental applications of magnetic measurements. *Science* **1980**, *207*, 481–486. [CrossRef]

29. Hunt, A.; Jones, J.; Oldfield, F. Magnetic measurements and heavy metals in atmospheric particulates of anthropogenic origin. *Sci. Total Environ.* **1984**, *33*, 129–139. [CrossRef]

30. Matzka, J.; Maher, B.A. Magnetic biomonitoring of roadside tree leaves: Identification of spatial and temporal variations in vehicle-derived particulates. *Atmos. Environ.* **1999**, *33*, 4565–4569. [CrossRef]

31. Hu, X.F.; Su, Y.; Ye, R.; Li, X.Q.; Zhang, G.L. Magnetic properties of the urban soils in Shanghai and their environmental implications. *Catena* **2007**, *70*, 428–436. [CrossRef]

32. Dearing, J.A.; Bird, P.M.; Dann, R.J.L.; Benjamin, S.F. Secondary ferrimagnetic minerals in Welsh soils: A comparison of mineral magnetic detection methods and implications for mineral formation. *Geophys. J. Int.* **1997**, *130*, 727–736. [CrossRef]

33. Fine, P.; Singer, M.J.; Verosub, K.L. Use of magnetic-susceptibility measurements in assessing soil uniformity in chronosequence studies. *Soil Sci. Soc. Am. J.* **1992**, *56*, 1195–1199. [CrossRef]

34. Fine, P.; Singer, M.J.; Verosub, K.L.; TenPas, J. New evidence for the origin of ferrimagnetic minerals in loess from China. *Soil Sci. Soc. Am. J.* **1993**, *57*, 1537–1542. [CrossRef]

35. Oldfield, F. Environmental magnetism—A personal perspective. *Quat. Sci. Rev.* **1991**, *10*, 73–85. [CrossRef]

36. Yang, M.; Li, H.M.; Li, F.Y.; Wang, J.H.; Diao, Y.W.; Qian, X.; Yang, Z.P.; Wang, C. Magnetic Response of Heavy Metal Pollution in Playground Dust of an Industrial Area. *Environ. Sci.* **2017**, *38*, 5282–5291.

37. Williams, W.; Dunlop, D.J. Simulation of magnetic hysteresis in pseudo-single-domain grains of magnetite. *J. Geophys. Res. Solid Earth* **1995**, *100*, 3859–3871. [CrossRef]

38. Maher, B. The magnetic properties of Quaternary aeolian dusts and sediments, and their palaeoclimatic significance. *Aeolian Res.* **2011**, *3*, 87–144. [CrossRef]

39. Winkler, A.; Amoroso, A.; Di Giosa, A.; Marchegiani, G. The effect of COVID-19 lockdown on airborne particulate matter in Rome, Italy: A magnetic point of view. *Environ. Pollut.* **2021**, *291*, 118191. [CrossRef]

40. Shanghai Municipal Bureau of Ecology and Environment. 2020. Available online: http://www.tianqihoubao.com/aqi/shanghai.html.website (accessed on 31 December 2020).

41. Gualtieri, G.; Brilli, L.; Carotenuto, F.; Vagnoli, C.; Zaldei, A.; Gioli, B. Quantifying road traffic impact on air quality in urban areas: A Covid19-induced lockdown analysis in Italy. *Environ. Pollut.* **2020**, *267*, 115682. [CrossRef]
42. Putaud, J.-P.; Pozzoli, L.; Pisoni, E.; Martins Dos Santos, S.; Lagler, F.; Lanzani, G.; Dal Santo, U.; Colette, A. Impacts of the COVID-19 lockdown on air pollution at regional and urban background sites in northern Italy. *Atmos. Chem. Phys.* **2021**, *21*, 7597–7609. [CrossRef]
43. The State Council of the People's Republic of China. *Three-Year Action Plan for Winning the Blue Sky Defense Battle*; The State Council of the People's Republic of China: Beijing, China, 2018.
44. Hansard, R.; Maher, B.; Kinnersley, R. Rapid magnetic biomonitoring and differentiation of atmospheric particulate pollutants at the roadside and around two major industrial sites in the UK. *Environ. Sci. Technol.* **2012**, *46*, 4403–4410. [CrossRef] [PubMed]
45. Chen, Y.; Zhang, W.; Dong, C.; Hutchinson, S.M.; Feng, H. Characteristics of iron-containing magnetic particles in household dust from an urban area: A case study in the megacity of Shanghai. *J. Hazard. Mater.* **2022**, *424*, 127212. [CrossRef] [PubMed]
46. Maher, B.; González-Maciel, A.; Reynoso-Robles, R.; Torres-Jardón, R.; Calderón-Garcidueñas, L. Iron-rich air pollution nanoparticles: An unrecognised environmental risk factor for myocardial mitochondrial dysfunction and cardiac oxidative stress. *Environ. Res.* **2020**, *188*, 109816. [CrossRef] [PubMed]
47. Chenery, S.R.; Sarkar, S.K.; Chatterjee, M.; Marriott, A.L.; Watts, M.J. Heavy metals in urban road dusts from Kolkata and Bengaluru, India: Implications for human health. *Environ. Geochem. Health* **2020**, *42*, 2627–2643. [CrossRef] [PubMed]
48. Wei, F.S.; Zheng, C.J.; Chen, J.S.; Wu, Y.Y. Study on the background contents on 61 elements of soils in China. *Environ. Sci.* **1991**, *12*, 12–19.
49. Han, Y.; Liu, X.; Zhao, G.; Lü, B.; Chen, Q. Magnetic monitoring of topsoil and street dust in Xinyang (China) and their environmental implications. *Environ. Monit. Assess.* **2021**, *193*, 602. [CrossRef]
50. Adamiec, E.; Jarosz-Krzemińska, E.; Wieszała, R. Heavy metals from non-exhaust vehicle emissions in urban and motorway road dusts. *Environ. Monit. Assess.* **2016**, *188*, 369. [CrossRef]
51. Men, C.; Liu, R.M.; Wang, Q.R.; Guo, L.J.; Shen, Z.Y. The impact of seasonal varied human activity on characteristics and sources of heavy metals in metropolitan road dusts. *Sci. Total Environ.* **2018**, *637*, 844–854. [CrossRef]
52. Zhao, X.; Yang, Y.; Guo, X. Pollution characteristics of heavy metals in atmospheric particulates from typical elevated highway in Changchun City. *Acta Sci. Circumst.* **2017**, *37*, 3280–3288.
53. Baba, A.; Gurdal, G.; Yucel, D.S. Enrichment of trace element concentrations in coal and its combustion residues and their potential environmental and human health impact: Can Coal Basin, NW Turkey as a case study. *Int. J. Environ. Technol. Manag.* **2016**, *19*, 455–480. [CrossRef]
54. Barbieri, M. The importance of enrichment factor (EF) and geoaccumulation index (Igeo) to evaluate the soil contamination. *J. Geol. Geophys.* **2016**, *5*, 237. [CrossRef]
55. Taghavi, S.N.; Kamani, H.; Dehghani, M.H.; Nabizadeh, R. Assessment of heavy metals in street dusts of Tehran using enrichment factor and geo-accumulation index. *Health Scope* **2019**, *8*, e57879. [CrossRef]
56. Chen, L.W.; Zhang, H.; Ding, M.J.; Devlin, A.T.; Wang, P.; Nie, M.H.; Xie, K. Exploration of the variations and relationships between trace metal enrichment in dust and ecological risks associated with rapid urban expansion. *Ecotoxicol. Environ. Saf.* **2021**, *212*, 111944. [CrossRef]
57. Dentener, F.J.; Carmichael, G.R.; Zhang, Y.; Lelieveld, J.; Crutzen, P.J. Role of mineral aerosol as a reactive surface in the global troposphere. *J. Geophys. Res. Atmos.* **1996**, *101*, 22869–22889. [CrossRef]
58. Ault, A.P.; Peters, T.M.; Sawvel, E.J.; Casuccio, G.S.; Willis, R.D.; Norris, G.A.; Grassian, V.H. Single-particle SEM-EDX analysis of iron-containing coarse particulate matter in an urban environment: Sources and distribution of iron within Cleveland, Ohio. *Environ. Sci. Technol.* **2012**, *46*, 4331–4339. [CrossRef]
59. Zhang, C.; Qiao, Q.; Appel, E.; Huang, B.C. Discriminating sources of anthropogenic heavy metals in urban street dusts using magnetic and chemical methods. *J. Geochem. Explor.* **2012**, *119*, 60–75. [CrossRef]
60. Chon, C.-M.; Park, J.-S.; Kim, J.-G.; Lee, Y.-S. Relationship between physicochemical properties, heavy metal contents and magnetic susceptibility of soils. *J. Mineral. Soc. Korea* **2010**, *23*, 281–295.
61. Zhu, Z.M.; Han, Z.X.; Bi, X.Y.; Yang, W.L. The relationship between magnetic parameters and heavy metal contents of indoor dust in e-waste recycling impacted area, Southeast China. *Sci. Total Environ.* **2012**, *433*, 302–308. [CrossRef]